

EXPERIMENTALLY ASSISTED MODELLING OF THE BEHAVIOUR OF STEEL ANGLE BRACE

A. M. BARSZCZ¹

Steel frame wind bracing systems are usually made of hot rolled profiles connected to frame elements directly or through a gusset plate. The behaviour of angle bracing members is generally complex since controlled by tension or compression, bending and torsion. The common practice is to transform the problem of complex behaviour into the buckling strength of a truss member. This paper deals with an analytical formulation of the force-deformation characteristic of a single angle brace subjected to compression. A strut model takes into consideration the effect of brace end connections and softening effect of its force-deformation characteristic. Two different boundary conditions, typical for engineering practice, are dealt with. Experimental program of testing the behaviour of angle brace in portal sub-frame specimens is described. Results of experimental investigations are presented. They are used for the validation of developed model. Conclusions are formulated with reference to the application of validated brace model in the analysis of braced steel frameworks.

Keywords: steel frame, truss bracing, angle brace, welded fork type connection, bolted through one leg type connection, force-deformation characteristic

1. INTRODUCTION

Many practical aspects of the strength prediction based on analytical modelling and experimental tests of single angle braces treated as an axially loaded members or beam-column type elements, in reference to their end connections, have already been researched, see Trahair et al. [1], Temple and Sakala [2], Elgaaly and Dawids [3], Alduri and Magudula [4], and Chan and Cho [5], among others. Ziemian [6] reviewed both experimental and analytical research work as well as summarized practical design concepts. Design methods are almost entirely based on the concept of equivalent slenderness that accounts for effects of both end connection eccentricities and restraints. Experimental study on equal/unequal leg angles subjected to eccentric compression was presented by Gizejowski et al. [7] and Lui and Chantel [8], among others. Recent developments are summarized by Chen and Wang [9,10].

¹ Faculty of Civil Engineering, Warsaw University of Technology, Poland,
e-mail: a.barszcz@il.pw.edu.pl

Another direction in investigations of the brace behaviour have been related to its force-deformation characteristic. Studies in the subject area were directed mainly towards the cyclic behaviour of compression elements of frame bracings in relation to collapse investigations of tall buildings in the seismic zone, see Ikeda and Mahin [11], Gan and Hall [12], Jin and El-Tawil [13], Fell et al. [14] and Davaran and Adelzadeh [15], among others. Furthermore, investigations were also carried out with regard to the elastic-plastic behavior of highly hyper-static spatial grid structures, see Łubiński et al. [16], Barszcz [17], Karczewski and Barszcz [18], Kato et al. [19], Ogawa et al. [20], Steinboeck et al. [21], in which buckling of a single strut does not generally lead to the immediate collapse of the whole system. The focus was made on modelling of the postbuckling range of deformations in order to trace the force redistribution process leading to the structure ultimate strength. Finally, methodology and techniques used for the description of cyclic behaviour of members in vertical bracing and spatial grid systems have been used for modelling of slender rebars in reinforced concrete systems, see Monti and Nuti [22], Dhakal and Maekawa [23], Korentz [24], among others.

Diagonals of truss bracings are traditionally designed for prebuckling compression or elastic tension. In case of X-type bracings, the members are designed as slender ones since they are not expected to resist buckling. As a result of such design, the compression diagonal buckles under compression and only the tension diagonal is considered to effectively resist sway. Although they are designed not to yield under tension they may buckle under compression, depending on the direction of horizontal forces. Such members are therefore subjected to changing deformation conditions. Compression brace elements, after reaching their buckling strength, do not maintain the ultimate strength level, as in case of yielded tension elements. The strength drop in the postbuckling region depends upon the brace slenderness, section type, grade of steel the member is made of and other factors among which the structural imperfections play an important role. Buckled members may be subjected to straightening out under the force reversal. If on this path the member is subjected to permanent deformations as a result of yielding in the straightening out phase, their reloading path is somewhat different from that of unloading path and the member is not able to reach the ultimate strength. The behaviour is a hysteretic type with its maximum force being dependent upon the amount of plastic deformations accumulated during the unloading phase.

For collapse behaviour of braced frame structures and the evaluation of their strength at the ultimate limit state, the investigations are usually restricted to one cycle behaviour of compression braces but carried out in such a way that for different section geometry, slenderness and steel grades, a developed simple analytical model could efficiently describe the equilibrium path of imperfect member in both prelimit and postlimit phases.

This paper presents the author's contribution to the development of a simple and yet accurate analytical model describing the equilibrium path of compressed angle braces. Two different boundary conditions of equal leg angle connections, typical for engineering practice, are dealt with, namely braces with welded fork type mono-eccentric

connections and braces with bolted lap through one leg bi-eccentric connections. Experimental program of testing the behaviour of angle braces in portal sub-frame specimens is described. Results of experimental investigations are presented and then used for the validation of developed analytical model of the brace behaviour. Finally, conclusions are formulated with reference to the application of validated brace model in the finite element analysis of braced steel frameworks.

2. BRACING MEMBER FORCE-DEFORMATION CHARACTERISTIC

2.1. FORCE-DEFORMATION CHARACTERISTIC OF A SINGLE IMPERFECT STRUT

The behaviour of compression brace is influenced by many factors among which the most important are: type of the element cross section that implies possible forms of elastic instability of perfect members, type of element material properties, geometric and material imperfections of real elements, see Murzewski [25]. Modelling techniques based on the Murzewski-Rankine-Merchant approach (M-R-M approach) for the behaviour prediction of compression members were presented by Barszcz and Gizejowski [26,27] and allowed for reproduction of the buckling curves of real compression members according to the Polish standard [28] and Eurocode 3 [29], respectively. Two approaches were specified, one that uses only the first-order elastic and plastic-strain-hardening mechanisms and the other one that uses all the first-order and second-order elastic and inelastic deformation mechanisms. The former approach allows only for the estimation of the real member ultimate strength in the similar way as the Shanley's theory of inelastic stability does. It does not however allow to describe the member force-deformation characteristic. The latter approach allows for the prediction of both the ultimate strength and the force-deformation characteristic of the compression member. This approach is utilized hereafter for modelling of the brace force-deformation characteristic of both connected centrally and eccentrically at end joints. Recalling the approach originally developed in [26,27], the characteristic generalized force-deformation relationship of an equivalent truss member of an arbitrary section can be written in the dimensionless format as follows:

$$(2.1) \quad \bar{\sigma} = \left(\bar{\sigma}_e^{-n} + \sum_{j \leq 2} \bar{\sigma}_{bf,j}^{-n} + \bar{\sigma}_{har}^{-n} + \bar{\sigma}_{ult}^{-n} \right)^{\frac{1}{n}}$$

where:

$\bar{\sigma}$ – dimensionless force ($= \frac{N_{Ek}}{\beta_A A f_y}$), N_{Ek} – characteristic axial force as an action effect,

$\beta_A = A_{eff}/A$ – effective section property factor (less than unity for class 4 sections

sensitive to elastic local buckling, otherwise equals to unity), A_{eff} – section effective area, A – section gross area, f_y – steel yield stress;

$\bar{\sigma}_E$ – dimensionless prebuckling force-deformation branch, linear according to the first order elastic theory for axially loaded members or nonlinear according to the second order theory for modelling the behaviour of eccentrically compressed members;

$\bar{\sigma}_{bif, j}$ – dimensionless bifurcation forces according to linear elastic stability theory, j – number of uncorrelated instability modes ($j = 2$ for bisymmetric section members for which deterministically independent are flexural and torsional modes, and for monosymmetric section members for which flexural in-plane and out-of-plane flexural-torsional modes are independent; $j = 1$ for asymmetric section members);

$\bar{\sigma}_{har}$ – dimensionless postyielding force-deformation branch, linear according to the first order plastic theory for material subjected to yielding and gradual hardening;

$\bar{\sigma}_{ult}$ – dimensionless postlimiting force-deformation branch, nonlinear according to the second order plastic hinge theory;

n – substitute imperfection parameters being, in the probabilistic modelling adopted, an inversion of the Weibull coefficient of variation.

Eqn. (2.1) allows for the evaluation of stiffness degradation model of an equivalent truss member. The tangent axial stiffness degradation factor $\bar{\kappa}$ describing the tangent axial stiffness $(EA)_t$ with regard to the member truss action can be calculated as follows:

$$(2.2) \quad \bar{\kappa} = \frac{d\bar{\sigma}}{d\bar{\varepsilon}} = \left[\bar{\sigma}_E^{-n} + \sum_{j \leq 2} \bar{\sigma}_{bif, j}^{-n} + \bar{\sigma}_{har}^{-n} + \bar{\sigma}_{ult}^{-n} \right]^{1+n} \left[\bar{\sigma}_E^{-n-1} \frac{d\bar{\sigma}_E}{d\bar{\varepsilon}} + \bar{\sigma}_{har}^{-n-1} \frac{d\bar{\sigma}_{har}}{d\bar{\varepsilon}} + \bar{\sigma}_{ult}^{-n-1} \frac{d\bar{\sigma}_{ult}}{d\bar{\varepsilon}} \right]$$

where:

$$\bar{\kappa} = \frac{(EA)_t}{EA}, \quad E - \text{modulus of elasticity.}$$

It is worth to note that bifurcation forces do not depend upon the dimensionless axial deformation $\bar{\varepsilon}$, therefore $\bar{\kappa}_{bif} = \frac{d\bar{\sigma}_{bif}}{d\bar{\varepsilon}} = 0$ and there are only three $\bar{\kappa}$ components in the second square bracket on RHS of Eqn. (2.2).

2.2. DEFORMATION MECHANISMS

In the following, the deformation mechanisms of angle brace in relation to the elastic prebuckling and buckling states as well as postyielding and postlimiting states are dealt with. The reference is made to Figure 1 where principal axes u and v coincide with the strong and weak section inertia axes, respectively and axis w is the brace member axis.

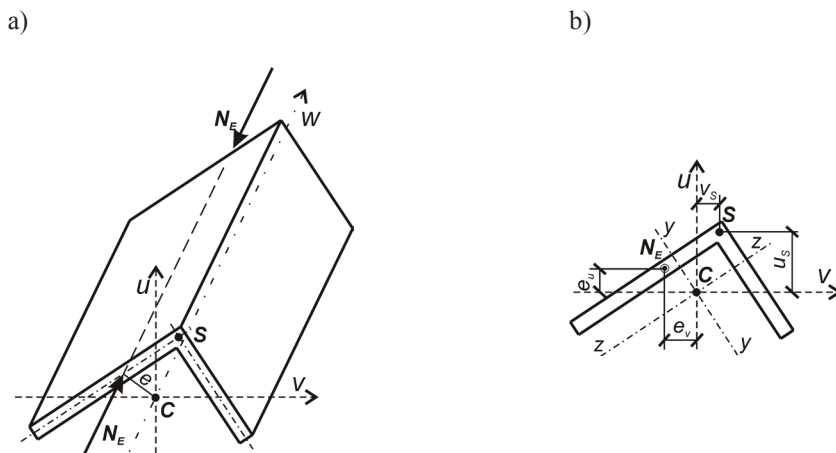


Fig. 1. Notation of section and member axes, shear centre (S) coordinates and axial action effect N_E eccentricities (C – gravity centre).

2.2.1. Elastic bifurcation mechanisms – $\bar{\sigma}_{bif,j}$

Calculation of bifurcation forces is discussed in details by Barszcz and Giżejowski [30]. They are derived from the theory of elastic stability of thin-walled members and their dimensionless counterparts are calculated as follows:

$$\bar{\sigma}_{bif,j} = \frac{N_{bif,j}}{\beta_A A f_y},$$

in which $N_{bif,j}$ are two forces or one force of the following bifurcation ones: flexural bifurcation force N_{Fu} or N_{Fv} , flexural-torsional bifurcation force N_{TFu} of compression in the plane of section symmetry $u-w$, torsional bifurcation force N_{Te} (or N_T) of compression with (or without) eccentricity with regard to shear centre S , and finally – general flexural-torsional bifurcation force N_{FT} ; β_A – effective section property factor as in Eqn. (2.1).

The general stability equation can be derived from the condition of zero determinant of the following matrix:

$$(2.3) \quad \mathbf{S} = \begin{bmatrix} N_{Fv} - N_{bif,j} & 0 & (u_S - e_u) N_{bif,j} \\ & N_{Fu} - N_{bif,j} & -(v_S - e_v) N_{bif,j} \\ \text{symm.} & & (N_{Te} - N_{bif,j}) i_S^2 \end{bmatrix}$$

here N_{Fv} , N_{Fu} and N_{Te} are the reference forces:

– N_{Fv} for flexural buckling about v axis:

$$N_{Fv} = \frac{\pi^2 EI_v}{(\mu_v l)^2}$$

– N_{Fu} for flexural buckling about u axis:

$$N_{Fu} = \frac{\pi^2 EI_u}{(\mu_u l)^2}$$

– N_{Te} for torsional buckling of eccentrically loaded member, about the member shear centre axis:

$$N_{Te} = \frac{GI_T}{i_S^2}$$

and I_v , I_u – section moments of inertia with reference to principal axes v and u , respectively; I_T – section Saint Venant torsion constant; G – modulus of rigidity; μ_v , μ_u – effective length factors for flexural buckling modes about axes v and u , respectively; l – system length, i_S – generalized polar radius of gyration of the eccentrically connected angle with respect to the shear centre S :

$$i_S^2 = i_T^2 \left(1 + \frac{e_u \beta_u + e_v \beta_v}{i_T^2} \right),$$

i_T – polar radius of gyration of centrally loaded angle with respect to the shear centre S :

$$i_T^2 = i_v^2 + i_u^2 + v_S^2 + u_S^2$$

i_v, i_u – radius of gyration of gross cross section about the axis v and u , respectively; β_v, β_u – cross-sectional properties associated with the Wagner effect for bending in principal planes:

$$\beta_v = \frac{1}{I_v} \left(\int_A u^3 dA + \int_A v^2 u dA \right) - 2u_S$$

$$\beta_u = \frac{1}{I_u} \left(\int_A v^3 dA + \int_A u^2 v dA \right) - 2v_S$$

The critical state is defined by the solution of matrix \mathbf{S} determinant equated to zero, i.e. $|\mathbf{S}| = 0$. The solution yields the algebraic equation of third degree with regard to $N_{bif, j}$. Its real value solution may be derived in a closed form solution as given in Appendix. Coefficients of the derived equation are as follows:

$$a = (u_S - e_u)^2 + (v_S - e_v)^2 - i_S^2,$$

$$b = i_S^2 (N_{Fv} + N_{Fu} + N_{Te}) - N_{Fv} (u_S - e_u)^2 - N_{Fu} (v_S - e_v)^2,$$

$$c = -i_S^2 [N_{Te} (N_{Fv} + N_{Fu}) + N_{Fv} N_{Fu}] \text{ and}$$

$$d = i_S^2 N_{Fv} N_{Fu} N_{Te}.$$

Only positive solutions are accounted for.

Different situations for angle section members are represented in Table 1. In the 5th column of Table 1 there are the components $\bar{\sigma}_{bif, j}$ need to be taken into consideration in the term $\sum_{j \leq 2} \bar{\sigma}_{bif, j}^{-n}$ of Eqn. (2.1). The following notation is applied: $\bar{\sigma}_{Fi}$ – dimensionless bifurcation force related to flexural mode about principal axis i , $\bar{\sigma}_{Te}$ – dimensionless bifurcation force related to torsional mode, $\bar{\sigma}_{TFi}$ – dimensionless bifurcation force related to the flexural mode out of the plane containing the axes i and w , $\bar{\sigma}_{TF}$ – dimensionless bifurcation force related to a general flexural-torsional mode of buckling.

The first terms N_{Fv} and N_{Fu} placed on the main diagonal of matrix \mathbf{S} given by Eqn. (2.3) are used for the approximation of second order elastic flexural deformations while the third term N_{Te} is to be used to approximate the axial stiffness (see a reduction factor ψ in the following section).

Table 1

Summary on how to choose parameters describing the force-deformation characteristic given by Eqn. (2.1) for an imperfect angle brace compressed axially or eccentrically

Angle	Case of compression	Identification of $\bar{\sigma}_E$	$\sum_{j \leq 2} \bar{\sigma}_{bif,j}^{-n}$		$\bar{\sigma}_{ult}$
			j	$\bar{\sigma}_{bif,j}$	m
Equal leg (monosymmetric) ²⁾	Eccentricity along axis u ; axial force at the shear center	$\bar{\sigma}_E$ from Eqn. (2.6a)	2	$\bar{\sigma}_{Fu}$ $\bar{\sigma}_{Te}^{1)}$	0,5
	Axial compression	$\bar{\sigma}_E = \bar{\varepsilon}$		$\bar{\sigma}_{Fv}$ $\bar{\sigma}_{TFu}$	
	Eccentricity along axis u ; axial force away from the shear center	$\bar{\sigma}_E$ from Eqn. (2.6)	1	$\bar{\sigma}_{TFu}$	1,0
	Eccentricity along axis v				
	Eccentricities along axes u and v	$\bar{\sigma}_E$ from Eqn. (2.8)		$\bar{\sigma}_{FT}$	
Unequal leg (asymmetric)	Eccentricities along axes u and v ; axial force at the shear center	$\bar{\sigma}_E$ from Eqn. (2.8)	1	$\bar{\sigma}_{Te}^{1)}$	1,0
	Axial compression	$\bar{\sigma}_E = \bar{\varepsilon}$		$\bar{\sigma}_{FT}$	
	Eccentricity along axis u or v	$\bar{\sigma}_E$ from Eqn. (2.6)			
	Eccentricities along axes u and v	$\bar{\sigma}_E$ from Eqn. (2.8)			

¹⁾ Considered only if $\bar{\sigma}_{Te} > 0$
²⁾ Plain of symmetry encompasses axis u

2.2.2. Elastic prebuckling deformation branch – $\bar{\sigma}_E$

- Centric compression (refer to [26,27])

The force-deformation characteristic:

$$(2.4) \quad \bar{\sigma}_E = \bar{\varepsilon}$$

where:

$$\bar{\varepsilon} = \varepsilon / (\beta_A \varepsilon_y),$$

$\varepsilon = \Delta / l$ – generalized normal strain, Δ – shortening due to axial compression, $\varepsilon_y = f_y / E$ – strain corresponding to the yield stress.

The stiffness degradation factor:

$$\bar{\kappa}_E = \frac{d\bar{\sigma}_E}{d\bar{\varepsilon}} = 1.$$

- Mono-eccentric compression

The elastic second order generalized stress $\bar{\sigma}_E$ is in this case the argument of a nonlinear inverse function $\bar{\varepsilon} = f(\bar{\sigma}_E)$. The deformation Δ for the evaluation of the generalized strain $\bar{\varepsilon}$ is of an additive format. It is the sum of the axial shortening as for the axially compressed member, refer to Eqn. (2.4), and shortening resulting from the bowing effect due to bending imposed on the member by axial forces applied through eccentric end connections. The relationship is established without solving the exact second order differential equilibrium equation but in an approximate way using the following assumptions:

- member deflected profile is of the parabolic form,
- second order deformation is calculated by using the amplification factor for the first order deformation component,
- effect of torsion on the axial stiffness in case of combined bending and torsion is approximated by using a reduction factor ψ .

The above assumptions yield for mono-eccentric compression the following relationships:

- eccentricity in the plane created by axes u and w :

$$(2.5a) \quad \bar{\varepsilon} = \frac{\bar{\sigma}_E}{\psi} + \frac{8E}{3f_y} \left(\frac{f_u^{II}}{l} \right)^2 = \frac{\bar{\sigma}_E}{\psi} + \frac{8E}{3f_y} \left(\frac{f_u^I}{l} \frac{1}{1 - \bar{\sigma}_E / \bar{\sigma}_{Fv}} \right)^2$$

- eccentricity in the plane created by axes v and w :

$$(2.5b) \quad \bar{\varepsilon} = \frac{\bar{\sigma}_E}{\psi} + \frac{8E}{3f_y} \left(\frac{f_v^{II}}{l} \right)^2 = \frac{\bar{\sigma}_E}{\psi} + \frac{8E}{3f_y} \left(\frac{f_v^I}{l} \frac{1}{1 - \bar{\sigma}_E / \bar{\sigma}_{Fu}} \right)^2$$

where:

$\bar{\sigma}_{Fv}$, $\bar{\sigma}_{Fu}$ – dimensionless flexural bifurcation forces about section principal axes v i u respectively, corresponding to the application of the axial force in the shear centre (refer to Figure 1) and all the stress quantities with bar over it are here and hereafter normalized with reference to the effective yield stress, e.g.

$$\bar{\sigma}_{Fi} = \frac{\sigma_{Fi}}{\beta_A f_y} = \frac{N_{Fi}}{\beta_A A f_y}$$

and N_{Fi} – forces related to the flexural bifurcation states about axes $i = u$ or $i = v$, f_i^I, f_i^{II} – first order and second order midspan deflections, e_i – eccentricity in the section principal axes $i = u$ or $i = v$.

Substituting in Eqn. (2.5) for f^I the member first-order maximum in-plane displacement coordinate calculated under the assumption of a parabolic member deflected profile, Eqns. (2.5) becomes the following ones:

$$(2.6a) \quad \bar{\varepsilon} = \frac{\bar{\sigma}_E}{\psi} + \frac{f_y}{24E} \left(\beta_A A l \frac{e_u}{I_v} \cdot \frac{\bar{\sigma}_E}{1 - \bar{\sigma}_E / \bar{\sigma}_{Fv}} \right)^2$$

$$(2.6b) \quad \bar{\varepsilon} = \frac{\bar{\sigma}_E}{\psi} + \frac{f_y}{24E} \left(\beta_A A l \frac{e_v}{I_u} \cdot \frac{\bar{\sigma}_E}{1 - \bar{\sigma}_E / \bar{\sigma}_{Fu}} \right)^2$$

Rearranging Eqns. (2.6a,b), the third degree algebraic equation with reference to $\bar{\varepsilon}$ is obtained that may be directly solved to get a closed form solution. These equations are thus rewritten to get the relationships as follows:

$$(2.7) \quad a\bar{\sigma}_E^{-3} + b\bar{\sigma}_E^{-2} + c\bar{\sigma}_E + d = 0$$

From all the cubic roots only those of real values obtained for the positive $\bar{\varepsilon}$ are considered. An analytical solution of such cubic equation is given in Appendix. The coefficients of this equation, namely a, b, c and d are dependent upon the plane of bending and are given by:

– eccentricity in the plane created by axes u and w :

$$\begin{aligned} a &= 24EI_v^2, \\ b &= \psi f_y \left(\beta_A A l e_u \bar{\sigma}_{Fv} \right)^2 - 24EI_v^2 \left(2\bar{\sigma}_{Fv} + \psi \bar{\varepsilon} \right), \\ c &= 24EI_v^2 \bar{\sigma}_{Fv} \left(\bar{\sigma}_{Fv} + 2\psi \bar{\varepsilon} \right), \text{ and} \\ d &= -24EI_v^2 \psi \bar{\varepsilon} \bar{\sigma}_{Fv}^2, \end{aligned}$$

– eccentricity in the plane created by axes v and w :

$$\begin{aligned} a &= 24EI_u^2, \\ b &= \psi f_y \left(\beta_A A l e_v \bar{\sigma}_{Fu} \right)^2 - 24EI_u^2 \left(2\bar{\sigma}_{Fu} + \psi \bar{\varepsilon} \right), \end{aligned}$$

$$c = 24EI_u^2 \bar{\sigma}_{Fu} (\bar{\sigma}_{Fu} + 2\psi \varepsilon), \text{ and}$$

$$d = -24EI_u^2 \psi \varepsilon \bar{\sigma}_{Fu}^2.$$

From roots belonging to the domain, only the positive real ones are further considered. Practically important are solutions based on the three roots of real values and the positive minimal one is considered for the analytical formulation of the brace force-deformation characteristic.

The stiffness degradation factor of considered elastic second order mechanism is derived as the first derivative of the solution of Eqn. (2.7), i.e. $\bar{\kappa}_E = \frac{d\bar{\sigma}_E}{d\varepsilon}$. It is given in

Appendix. Moreover, the following notation is used herein:

- for eccentricity in the plane created by axes u and w :

$$b' = -24\psi EI_v^2, \quad c' = 48\psi EI_v^2 \bar{\sigma}_{Fv}, \quad d' = -24\psi EI_v^2 \bar{\sigma}_{Fv}^2,$$

- eccentricity in the plane created by axes v and w :

$$b' = -24\psi EI_u^2, \quad c' = 48\psi EI_u^2 \bar{\sigma}_{Fu}, \quad d' = -24\psi EI_u^2 \bar{\sigma}_{Fu}^2.$$

The stiffness reduction factor ψ is equal to unity for axially loaded braces and braces with a single eccentricity causing an equal leg angle brace to bend without torsion (bending in the plane of section symmetry, i.e. about the weak axis). For mono-eccentric compression about the strong axis and compression with double eccentricities, bending is associated by torsion and the stiffness reduction factor $\psi \leq 1$.

- Bi-eccentric compression

The elastic second order deformation $\bar{\sigma}_E$ is in this case set up as a nonlinear inverse function $\varepsilon = f(\bar{\sigma}_E)$ in the similar way as for the mono-eccentric compression. The dimensionless form of this inverse function is given by:

$$(2.8) \quad \bar{\varepsilon} = \frac{\bar{\sigma}_E}{\psi} + \frac{8E}{3f_y} \left[\left(\frac{f_u^{\text{II}}}{l} \right)^2 + \left(\frac{f_v^{\text{II}}}{l} \right)^2 \right] = \frac{\bar{\sigma}_E}{\psi} + \frac{8E}{3f_y l^2} \left[\left(\frac{f_u^{\text{I}}}{1 - \bar{\sigma}_E / \sigma_{Fv}} \right)^2 + \left(\frac{f_v^{\text{I}}}{1 - \bar{\sigma}_E / \sigma_{Fu}} \right)^2 \right] =$$

$$= \frac{\bar{\sigma}_E}{\psi} + \frac{f_y}{24E} (\beta_A A l)^2 \left[\left(\frac{e_u}{I_v} \cdot \frac{\bar{\sigma}_E}{1 - \bar{\sigma}_E / \sigma_{Fv}} \right)^2 + \left(\frac{e_v}{I_u} \cdot \frac{\bar{\sigma}_E}{1 - \bar{\sigma}_E / \sigma_{Fu}} \right)^2 \right]$$

Rearranging Eqn. (2.8), the following fifth degree algebraic equation is obtained:

$$\begin{aligned}
 & 24E(I_v I_u)^2 \bar{\sigma}_E^5 + \\
 & + \left\{ \psi f_y (\beta_A A I)^2 \left[(I_u e_u \bar{\sigma}_{Fv})^2 + (I_v e_v \bar{\sigma}_{Fu})^2 \right] - 24E(I_v I_u)^2 \left[2\bar{\sigma}_{Fv} + 2\bar{\sigma}_{Fu} + \psi \varepsilon \right] \right\} \bar{\sigma}_E^4 \\
 & + 2 \left\{ 12E(I_v I_u)^2 \left[\bar{\sigma}_{Fu}^2 + 4\bar{\sigma}_{Fu} \bar{\sigma}_{Fv} + \bar{\sigma}_{Fv}^2 + 2\psi \varepsilon (\bar{\sigma}_{Fu} + \bar{\sigma}_{Fv}) \right] + \right. \\
 (2.9) \quad & - \psi f_y (\beta_A A I)^2 \bar{\sigma}_{Fv} \bar{\sigma}_{Fu} \left[(I_u e_u)^2 \bar{\sigma}_{Fv} + (I_v e_v)^2 \bar{\sigma}_{Fu} \right] \left. \right\} \bar{\sigma}_E^3 \\
 & + \left\{ \psi f_y (\beta_A A I \bar{\sigma}_{Fv} \bar{\sigma}_{Fu})^2 \left[(I_u e_u)^2 + (I_v e_v)^2 \right] + \right. \\
 & - 24E(I_v I_u)^2 \left[\psi \varepsilon (\bar{\sigma}_{Fu}^2 + 4\bar{\sigma}_{Fu} \bar{\sigma}_{Fv} + \bar{\sigma}_{Fv}^2) + 2\bar{\sigma}_{Fu} \bar{\sigma}_{Fv} (\bar{\sigma}_{Fu} + \bar{\sigma}_{Fv}) \right] \left. \right\} \bar{\sigma}_E^2 \\
 & + 24E(I_v I_u)^2 \bar{\sigma}_{Fu} \bar{\sigma}_{Fv} \left[2\psi \varepsilon \bar{\sigma}_{Fu} + 2\psi \varepsilon \bar{\sigma}_{Fv} + \bar{\sigma}_{Fu} \bar{\sigma}_{Fv} \right] \bar{\sigma}_E \\
 & - 24\psi E \varepsilon (I_v I_u)^2 \bar{\sigma}_{Fu}^2 \bar{\sigma}_{Fv}^2 = 0
 \end{aligned}$$

The domain of $\bar{\sigma}_E$ roots of the above equation considered hereafter is limited to real and positive values lesser than $\bar{\sigma}_E = \min(\bar{\sigma}_{Fu}, \bar{\sigma}_{Fv})$. Solving the fifth degree equation by hand is rather complex so that one has to resort to numerical methods. The same is applied for the axial stiffness degradation factor $\bar{\kappa}_E = \frac{d\bar{\sigma}_E}{d\varepsilon}$.

For bi-eccentric compression, bending moments are associated by torsion and the stiffness reduction factor $\psi \leq 1$. The following interpolation formula is suggested to approximately account for the reduction of axial stiffness due to torsion:

$$(2.10) \quad \psi = \frac{c_1}{c_1 + c_2 \frac{N_F}{N_{Te}}}$$

where: c_1, c_2 – constants to be adjusted, $N_F = \min(N_{Fv}, N_{Fu})$, N_{Te} – torsional force, see Eqn. (2.3), but provided that:

$$N_{Te} \geq N_T = \frac{GI_T}{i_T^2}$$

In the third column of Table 1 there is an identification of terms used for the determination of $\bar{\sigma}_E$ for angle braces subjected to axial, monoaxial and biaxial compression.

It is important to note that for angle struts unrestrained between end supports and having real positive bifurcation forces, the following relationship holds:

$$(2.11) \quad \bar{\sigma}_{cr} \leq \min(\bar{\sigma}_F, \bar{\sigma}_{Te})$$

where: $\bar{\sigma}_{Te}$ – dimensionless torsional bifurcation force:

$$\bar{\sigma}_{Te} = \frac{N_{Te}}{\beta_A A f_y},$$

and $\bar{\sigma}_{cr} = \min \bar{\sigma}_{bif,j}$ – dimensionless critical force understood hereafter as the minimum value of bifurcation forces from all the deterministically possible modes of buckling.

Considering Eqn. (2.11), one may suggest two possible simplifications of Eqn. (2.8):

– the first higher approximation:

$$(2.12) \quad \bar{\varepsilon} \approx \frac{\bar{\sigma}_E}{\psi} + \frac{8E}{3f_y} \left[\left(\frac{f^I}{l} \frac{1}{1 - \bar{\sigma}_E/\bar{\sigma}_F} \right)^2 \right]$$

– the second lower approximation:

$$(2.13) \quad \bar{\varepsilon} \approx \frac{\bar{\sigma}_E}{\psi} + \frac{8E}{3f_y} \left[\left(\frac{f^I}{l} \frac{1}{1 - \bar{\sigma}_E/\bar{\sigma}_{cr}} \right)^2 \right]$$

where: $f^I = \sqrt{f_u^{I^2} + f_v^{I^2}}$ – resultant midspan deflection.

Figure 2 illustrates the accuracy of approximations given by Eqns. (2.12) and (2.13) in relation to a more exact relationship (2.8). An unequal angle of 120x80x10 and three lengths 1m, 2m and 3m are considered, and for the simplicity of comparison the axial stiffness reduction factor $\psi = 1$ is used for this comparison. Two cases of bi-eccentric compression are accounted for, namely the connection through the longer leg (Figure 2a) and through the shorter leg (Figure 2b), and the gravity center of bolt connectors is taken as recommended in tables of angle rolled products. In the former case it is placed

at 65 mm from the angle corner along the leg axis parallel to the section $z-z$ axis (see Figure 1), and the latter – at 45 mm the angle corner along the leg axis parallel to the section $y-y$ axis (see Figure 1). In order to normalize stress and strain quantities, the yield stress of steel grade S355 is used. It is important to note that in the former case, the approximation according to Eqn. (2.12) creates the closer solution to the original equation (2.8) than in the latter case based on Eqn. (2.13).

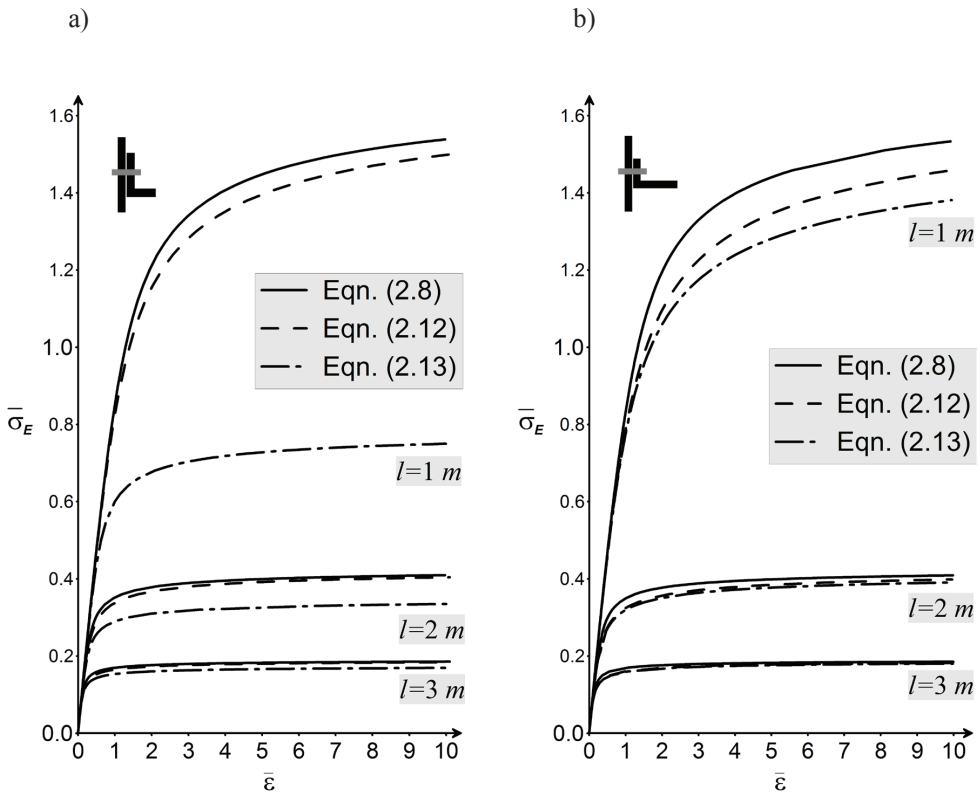


Fig. 2. Comparison of dimensionless elastic second order force-deformation characteristic for a chosen unequal angle brace for its three lengths; a) angle connected through the longer leg, b) angle connected through the shorter leg.

The advantage of simplifications of Eqns. (2.12) and (2.13) is that they lead to the reduction of the fifth degree algebraic Eqn. (2.8) to the cubic equation similar to that of Eqn. (2.7) that may easily be solved by hand. It is however clear from Figure 2 that both approximations do not generally fit well the more exact solution. The first approximation, according to Eqn. (2.12), is in Figure 2a closer to the “exact one” (2.8) while in Figure 2b it is closer to the second approximation (2.13), instead to the “exact one”

(2.8). Since both possible simplifications do not give sufficiently accurate modeling of the angle brace force-deformation characteristic in a wide range of practically met strut lengths and angle orientations, more accurate relationship (2.9) is maintained hereafter for the evaluation of $\bar{\sigma}_E$ and modelling of the angle brace behaviour.

2.2.3. Deformation postyielding mechanism – $\bar{\sigma}_{har}$

Inelastic first order deformations of an angle made of elastic-rigid-plastic material with linear isotropic hardening is expressed as follows:

$$(2.14) \quad \bar{\sigma}_{har} = 1 + \alpha_h \bar{\varepsilon}$$

where:

α_h – hardening modulus factor.

The stiffness degradation factor is of a constant value because of a linear form of Eqn. (2.14):

$$\bar{\kappa}_{har} = \frac{d\bar{\sigma}_{har}}{d\bar{\varepsilon}} = \alpha_h.$$

2.2.4. Postlimiting deformation mechanism – $\bar{\sigma}_{ult}$

The mechanism considered herein describe the brace behaviour after formation of the plastic hinge in the most stressed brace section. The corresponding relationship for plane buckling is derived in [26,27] and can be rewritten as:

$$(2.15) \quad \bar{\sigma}_{ult} = \frac{1}{a_u \left(\frac{\bar{\varepsilon}}{\sigma_F} \right)^m}$$

where:

a_u – section shape factor that is treated as an equivalent shape factor in Eqn. (2.1), the value of which is a constant dependent on the section type and type of prebuckling deformations,

m – parameter for compressed braces (0,5 for axially compressed members [26,27]).

The parameter $m = 0,5$ holds also for angles with the eccentric compression in the plane of section symmetry and it is postulated hereafter to adopt $m=1,0$ otherwise (refer to the 6th column of Table 1).

The stiffness degradation factor takes therefore the following form:

$$(2.16) \quad \bar{\kappa}_{ult} = \frac{d\bar{\sigma}_{ult}}{d\bar{\varepsilon}} = -\frac{m}{a_u \left(\frac{\bar{\varepsilon}}{\sigma_F} \right)^m \bar{\varepsilon}}$$

2.3. SUMMARY OF ACCURACY OF ADOPTED APPROXIMATIONS

Figure 3 illustrates the influence on the force-deformation characteristic given by Eqn. (2.1) of following approximations:

- utilization of Eqns. (2.12) and (2.13) instead of the “exact” relationship (2.8),
- omission of the interaction effect of flexural and torsional modes of buckling by the modification of RHS second term in the bracket of Eqn. (2.1).

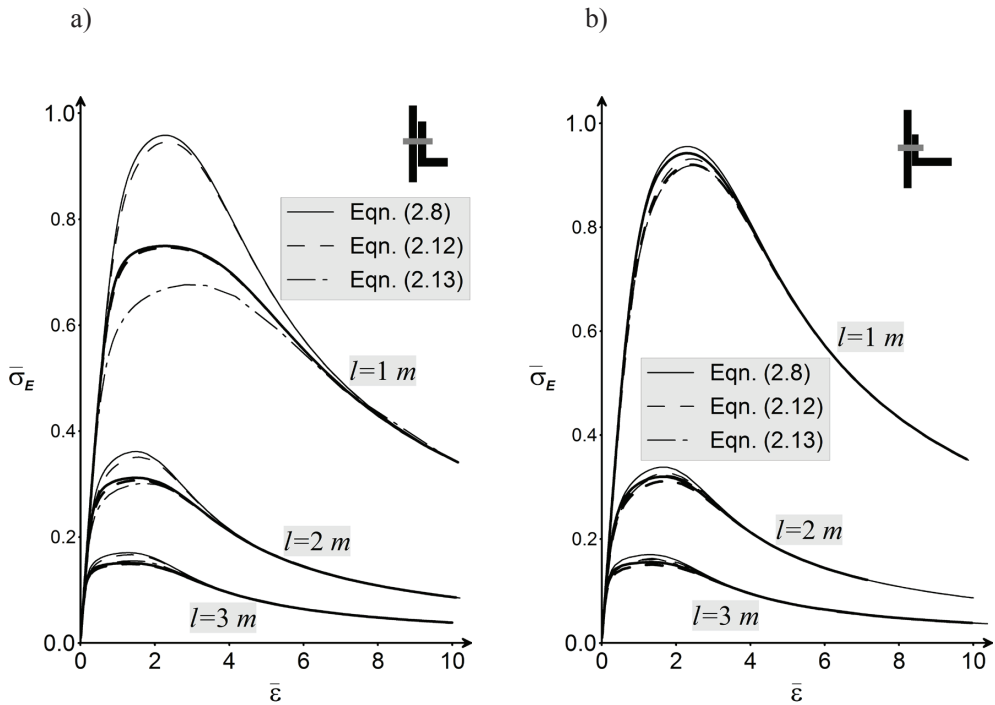


Fig. 3. Comparison of force-deformation characteristics for a chosen unequal angle brace from Figure 2 made of a higher steel grade; a) angle connected through the longer leg, b) angle connected through the shorter leg.

Omitting the interaction effect, the RHS second term in the bracket of Eqn. (2.1) is neglected and all the buckling effects are accounted for by using the second order equations (2.12) or (2.13) instead of Eqn. (2.8). Including the above effect, the said term is maintained, the approximation is referred to using Eqn. (2.12) instead of Eqn. (2.8).

The comparison is given in Figure 3 for the same exemplary angle section as considered in Figure 2. The same steel grade is adopted. Thick lines represent the situation

when the interaction effect is considered, i.e. the term $\sum_{j \leq 2} \bar{\sigma}_{bif,j}^{-n}$ included in Eqn. (2.1).

Thin lines represent the situation when the interaction effect is neglected, i.e. the term

$\sum_{j \leq 2} \bar{\sigma}_{bif,j}^{-n}$ omitted in Eqn. (2.1). The solid line represents the application of „exact” second

order equation (2.8) while the other two lines – the application of its approximations, namely given by Eqn. (2.12) – a discontinuous line, by Eqn. (2.13) – a discontinuous and dotted line. It is clear from Figure 3 that two possible ways of simplifications do not give sufficiently accurate modelling of the angle brace force-deformation characteristic in a range of practically important strut lengths. Generally, in case of longer angle members, the differences are lesser. The conclusion is that possible approximations lead to a different degree of accuracy with regard of the most accurate one identified by the

inclusion of term $\sum_{j \leq 2} \bar{\sigma}_{bif,j}^{-n}$ in Eqn. (2.1) and the second order flexural approximation of the relationship $\bar{\sigma}_E - \bar{\varepsilon}$ given by Eqn. (2.8).

3. SPECIAL CASES OF EQUAL LEG ANGLE BRACE

The modelling technique presented in section 2 for a general case of unequal leg angle brace is used hereafter for the development of force-deformation characteristic of equal leg angle brace and its validation with use of experimental results into the brace behaviour based on tests on braced portal subframes. Subframe arrangements included two types of brace end joints that created two different ways of axial force transfer from the brace onto the frame columns the brace was attached to, namely fork welded and single leg bolted. These joint details correspond to two different model situations that are marked in Table 1 by grey colour. The case of fork welded joint corresponds to the application of the axial force in the plane of section symmetry but away from the gravity centre C , while the single leg bolted joint corresponds to the application of the axial force at the bolt group gravity centre that is placed at the interface between the connected leg and the gusset plate, out of the plane of section symmetry as well as away from the gravity centre C and shear centre S .

3.1. BRACE WITH FORK WELDED END JOINTS

The case of angle bracing member with an in-plane eccentricity is shown in Figure 4. This is a typical case for a single angle bracing member connected by welding through a gusset plate to the frame load bearing system. An eccentricity appears in the plane of section symmetry and the deflection is imposed along axis u as described by Eqn. (2.6a).

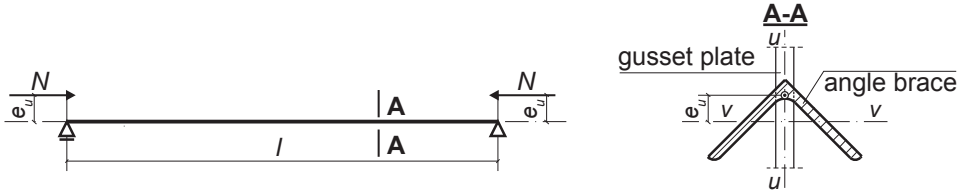


Fig. 4. Eccentrically connected angle bracing member subjected to in-plane bending and compression.

Since Eqn. (2.6a) accounts for the flexural bifurcation force in the plane of section symmetry (about axis $v-v$), summation in the third RHS term in the bracket of Eqn. (2.1) simplifies to that of flexural-torsional bifurcation force with the mode characterized by flexural deflections out of the plane of section symmetry (about axis $u-u$) with the simultaneous rotation about member axis. Dimensionless bifurcation force σ_{FuT} is calculated using the well known relationship:

$$(3.1) \quad \bar{\sigma}_{TFu} = \frac{(\bar{\sigma}_{Fu} + \bar{\sigma}_{Te}) - \sqrt{(\bar{\sigma}_{Fu} + \bar{\sigma}_{Te})^2 - 4\bar{\sigma}_{Fu}\bar{\sigma}_{Te} \left[1 - \mu(u_s - e_u)^2 / i_s^2 \right]}}{2 \left[1 - \mu(u_s - e_u)^2 / i_s^2 \right]}$$

where:

$\bar{\sigma}_{Fu}, \bar{\sigma}_{Te}$ – dimensionless reference forces corresponding to the bifurcation ones when the axial force acts in the plane of section symmetry, i.e.

- flexural about axis $u-u$, $\bar{\sigma}_{Fu} = 1 / \bar{\lambda}_{Fu}^2$, where: $\bar{\lambda}_{Fu} = \lambda_{Fu} / \lambda_1$ – non-dimensional member slenderness for flexural in-plane buckling about the axis u , $\lambda_{Fu} = \lambda_u / i_u$ – member slenderness ratio, $\lambda_1 = \pi \sqrt{E / \beta_A f_y}$ – comparative slenderness,
- torsional about the member shear centre axis, $\bar{\sigma}_{Te} = \frac{GI_T}{Af_y i_S^2}$, where:

$$i_S^2 = i_T^2 \left(1 + \frac{e_u \beta_u}{2 i_T^2} \right), \quad i_T^2 = i_u^2 + i_v^2 + u_S^2.$$

The relative slenderness ratio corresponding to Eqn. (3.1) is of the form: $\bar{\lambda}_{TFu} = 1/\sqrt{\bar{\sigma}_{TFu}}$.

The brace governing relative slenderness $\bar{\lambda} = \max(\bar{\lambda}_{Fv}, \bar{\lambda}_{TFu})$ is generally dependent upon the length of the member and steel yield strength ($\bar{\lambda}_{Fv} = \lambda_{Fv}/\lambda_1 = \mu_v l/i_v/\lambda_1$). For common steel grades and brace lengths of the most practical applications, there is $\bar{\lambda} = \bar{\lambda}_{Fv}$. However case $\bar{\lambda} = \bar{\lambda}_{TFu}$ might govern buckling of high strength steel grades that are nowadays more and more popular.

For eccentricity only in the plane of section symmetry $m = 0,5$, $\bar{\sigma}_F = \bar{\sigma}_{Fv} = 1/\bar{\lambda}_{Fv}^2$ and Eqn. (2.15) takes the form:

$$\bar{\sigma}_{ult} = \frac{1}{a_u \bar{\lambda}_{Fv} \sqrt{\varepsilon}},$$

as well as Eqn. (2.16) becomes of the following format:

$$\bar{\kappa}_{ult} = -\frac{1}{2a_u \bar{\lambda}_{Fv} (\sqrt{\varepsilon})^3}.$$

3.2. BRACE WITH BOLTED THROUGH ONE LEG END JOINTS

The case of equal leg angle bracing member bolted through one leg to the frame load bearing system is shown in Figure 5. The similar considerations apply when the angle leg is fillet welded to the gusset plate. The only difference is that the gravity centre of the connector group through which the axial force is being transferred from the bracing element onto the frame element might be in a different place. The maximum bolt diameter and the placement of bolt rows along the angle leg is given in the table of rolled angle products. It determines the position of the gravity centre of the bolt group. The gravity centre position of the connector group in case of fillet welds is however in a wider range since there might be a number of fillet weld group arrangements. In both cases therefore, the axial force transfer through the connection is associated with eccentricity components along two sectional axes. Thus, bending associated with these eccentricity components results in flexural deflection components in both planes and torsion.

Elastic prebuckling deformation branch $\bar{\sigma}_E - \bar{\varepsilon}$ is described by Eqns. (2.8) and (2.9). The domain of Eqn. (2.9) is $\bar{\varepsilon} \geq 0$ and for the solutions evaluated numerically that have the physical sense, i.e. $\bar{\sigma}_E < \bar{\sigma}_F$ or in terms of slenderness ratios: $\bar{\sigma}_E < \min(1/\bar{\lambda}_{Fv}^2, 1/\bar{\lambda}_{Fu}^2)$.

Critical state of the bi-eccentrically compressed strut is of a space nature. The dimensionless critical force $\bar{\sigma}_{FT}$ is evaluated by solving the determinant of **S** matrix given by Eqn. (2.3). The following cubic algebraic equation is obtained:

$$(3.2) \quad (\bar{\sigma}_{Fu} - \bar{\sigma}_{FT})(\bar{\sigma}_{Fv} - \bar{\sigma}_{FT})(\bar{\sigma}_{Te} - \bar{\sigma}_{FT}) - (\bar{\sigma}_{Fu} - \bar{\sigma}_{FT})\bar{\sigma}_{FT}^2(v_S - e_v)^2/i_S^2 + \\ - (\bar{\sigma}_{Fv} - \bar{\sigma}_{FT})\bar{\sigma}_{FT}^2(u_S - e_u)^2/i_S^2 = 0$$

After rearranging, Eqn. (3.2) takes the form of algebraic equation:

$$a\bar{\sigma}_{FT}^3 + b\bar{\sigma}_{FT}^2 + c\bar{\sigma}_{FT} + d = 0,$$

the solution of which is given in Appendix where x is replaced by $\bar{\sigma}_{FT}$, and the coefficients a , b , c and d are as follows:

$$a = (v_S - e_v)^2 + (u_S - e_u)^2 - i_S^2, \quad b = i_S^2(\bar{\sigma}_{Fu} + \bar{\sigma}_{Fv} + \bar{\sigma}_{Te}) - (v_S - e_v)^2\bar{\sigma}_{Fu} - (u_S - e_u)^2\bar{\sigma}_{Fv}, \\ c = -i_S^2[(\bar{\sigma}_{Fv} + \bar{\sigma}_{Fu})\bar{\sigma}_{Te} + \bar{\sigma}_{Fu}\bar{\sigma}_{Fv}], \quad d = i_S^2\bar{\sigma}_{Fu}\bar{\sigma}_{Fv}\bar{\sigma}_{Te}.$$

Only positive roots are considered and if there are more than one positive roots, the minimal positive root defines the critical state.

For the postlimit deformation mechanism in case of bi-eccentric bending about principal axes $m = 1$, $\bar{\sigma}_F = \min(1/\bar{\lambda}_{Fv}^2, 1/\bar{\lambda}_{Fu}^2)$ and Eqn. (2.15) takes the form:

$$\sigma_{ult} = \frac{1}{a_u \bar{\lambda}_F^2 \varepsilon},$$

therefore the stiffness degradation factor is of the following format:

$$\bar{K}_{ult} = -\frac{1}{a_u \bar{\lambda}_F^2 \varepsilon}.$$

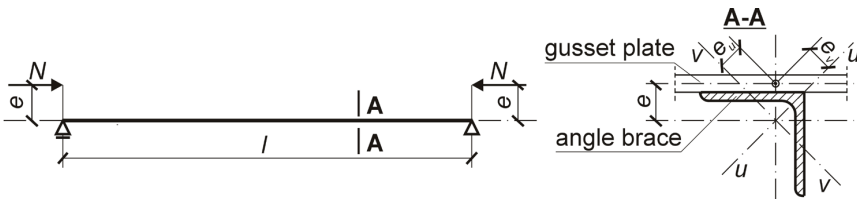


Fig. 5. Eccentrically connected angle bracing member subjected to space bending, torsion and compression.

3.3. COMPARISON OF FORCE-DEFORMATION CHARACTERISTICS AND STIFFNESS DEGRADATION FACTORS FOR COMPRESSED ANGLE BRACES WITH DIFFERENT END CONNECTIONS

In order to compare the force-deformation characteristics of imperfect angle brace, the results obtained for the brace with a single in-plane eccentricity (welded end connections) and the brace with a space in-plane and out-of-plane eccentricity components (bolted end connections through one leg) are presented. A single in-plane eccentricity of welded brace end connections results in a drop of the ultimate strength the magnitude of which is dependent upon the value of eccentricity. A space eccentricity of bolted brace end connections results in a further drop of the ultimate strength but also in a different response in the postlimit range. This is attributed to the integrated effect of bending in two directions and torsion affecting the behaviour in the elastic and plastic regions.

Figure 6 illustrates the force-deformation characteristics for an equal leg angle 60x60x5 that is considered hereafter for validation of the developed model. Solid discontinuous lines represent the upper bound deterministic solution while its solid continuous counterpart represents the probabilistic solution through Eqn. (2.1). The following parameters are used: for stocky brace $\bar{\lambda} = \bar{\lambda}_{F_v} = 0,5$ and for slender brace $\bar{\lambda} = \bar{\lambda}_{F_v} = 2,0$. In addition, the eccentricity of $e_u=10\text{mm}$ or fork welded connection and $e_u = 2 \text{ mm}$ and $e_v = 28 \text{ mm}$ for a single leg bolted connection. Moreover the following parameters are used: $\alpha_h = 0,02$; $a_u = 1$ as well as $n=5$ for welded connections and $n=3,5$ for bolted connections.

Figure 7 illustrates the upper bound deterministic tangent axial stiffness factor $\bar{\kappa}$ relationship and its probabilistic counterpart for a brace connections of which result in in-plane eccentricity. The same parameters are used as for construction of force-deformation characteristics given in Figure 6. It is important to note that all the elementary deformation mechanisms that are decisive from the point of view of the probabilistic concept of the imperfect brace characteristic are considered.

4. EXPERIMENTAL INVESTIGATIONS

Experimental investigations have been conducted by the author in the recent years in the Laboratory of the Metal Structures Department of the Warsaw University of Technology and presented in [31] with regard to the pilot tests and in [32] with regard to the results of the main tests. A brief description of the specimens used, testing stand and testing procedure applied is presented in [33] and followed by the presentation of test results in the form that is directly utilized in the calibration of developed analytical model.

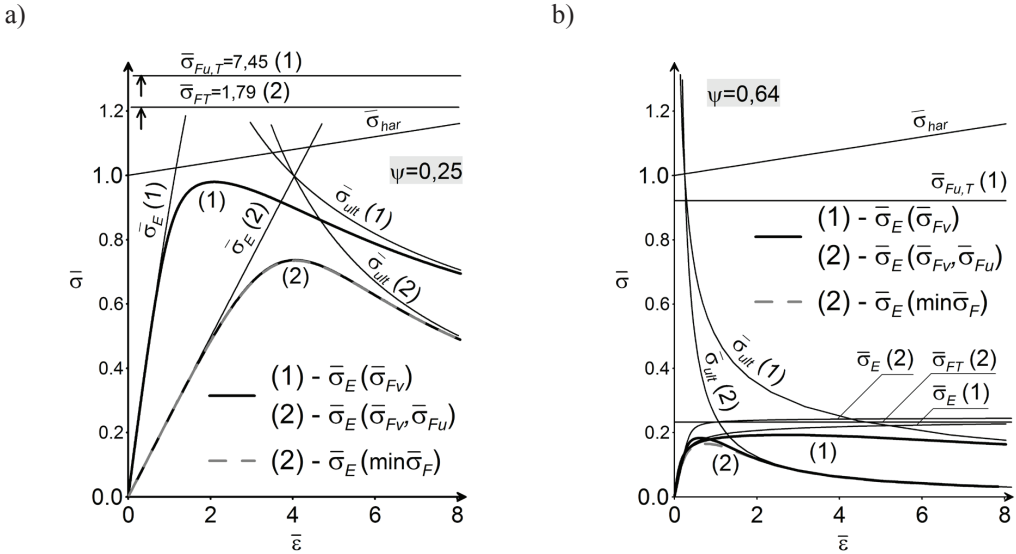


Fig. 6. Comparison of dimensionless deterministic and probabilistic force-deformation characteristics of angle brace using the parameters: $\alpha_h = 0,02$, $a_u = 1$, and (1) – in-plane eccentricity for which $e_u = 10$ mm, $n = 5$, (2) – space eccentricity for which $e_u = 2$ mm, $e_v = 28$ mm, $n = 3,5$; a) stocky angle $\bar{\lambda}_{Fv} = 0,5$, b) slender angle $\bar{\lambda}_{Fv} = 2,0$.

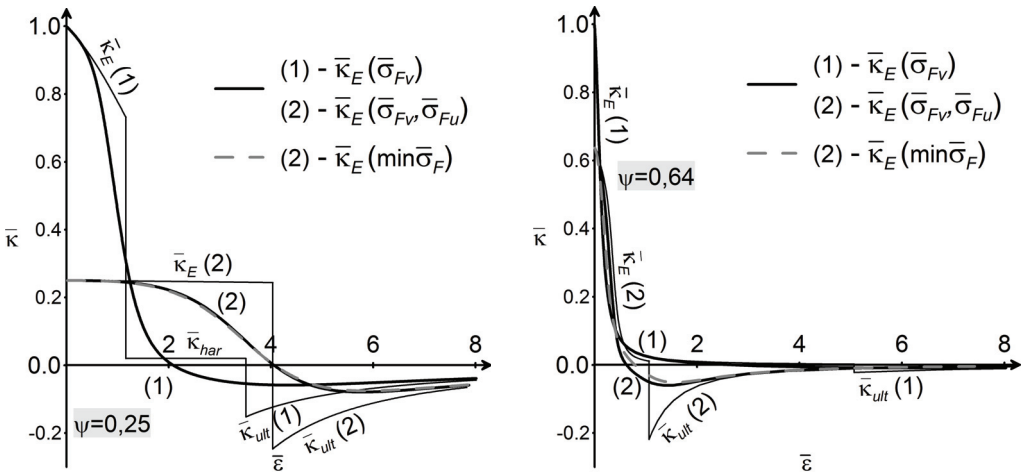


Fig. 7. Comparison of deterministic and probabilistic tangent axial stiffness of eccentrically connected brace corresponding to force-deformation characteristics from Figure 6; a) stocky angle $\bar{\lambda}_{Fv} = 0,5$, b) slender angle $\bar{\lambda}_{Fv} = 2,0$.

4.1. BRIEF DESCRIPTION OF SPECIMENS AND TESTING PROCEDURE

The main test series contained 19 braced portal frame subassemblages divided into 2 groups of specimens. The first group consisted of 3 subgroups of specimens with angle braces welded to the main frame through a gusset plate and being differentiated by the length of angle braces (their slenderness). The brace end connections were concentric about the plane of the frame but with in-plane eccentricity (see Figure 8). Welds were extended along the fork length of angle legs.

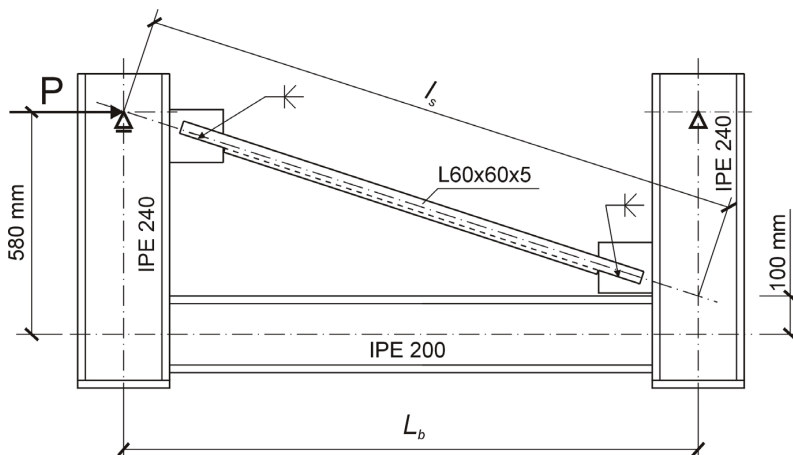


Fig. 8. Geometry of portal frame specimens of group WL (side view) [33].

The second group consisted of 3 subgroups of specimens with angle braces bolted to the main frame through a gusset plate and being differentiated by the length of angle braces in the same way as for the specimens of group 1. The brace end connections were arranged as leg-to-gusset joints with space eccentricity (see Figure 9). Two bolt connectors of M16 and class 6.6(5) were used for each end brace connection and designed in such a way that the bolt failure was not a governing strength criterion for the brace. Table 2 gives the symbols used to distinguish the frame specimens according to the beam system length.

Sub-frame specimens were tested upside down. One of the supports was moveable and subjected to the horizontal travel of the jack piston while the other support was immovable and attached to the rigid stand.

Beam-to-column joints are fillet welded and arranged in such a way that they are independent from the connection of bracing member. The brace axis coincides with both the column axis and the line of applied load at the top while at the bottom has an eccentricity with reference to the beam-to-column joint, see Figures 8 and 9.

Sizes of frame members for two groups of tested subassemblages were chosen in such a way that the brace is a weakest component within the frame members. The frame

verticals are made of IPE 240 rolled I-profiles and connected to the horizontal one made of IPE 200 rolled I-profile through semi-rigid joints (unstiffened welded joints). The brace member section was a 60x60x5 rolled equal leg angle. Semi-rigid beam-to-column joints are fillet welded and arranged in such a way that they are independent from bracing member joints. Gusset plates of 10mm in thickness were welded to the frame verticals. Frame I-profiles and gusset plates were made of steel grade S235JR2. Material testing was performed for coupons cut from profiles used for manufacturing of test specimens. There were two deliveries of specimen profiles so that two series of mechanical properties of steel grades used were conducted. The mechanical properties of steel grade from material testing are given in Table 3.

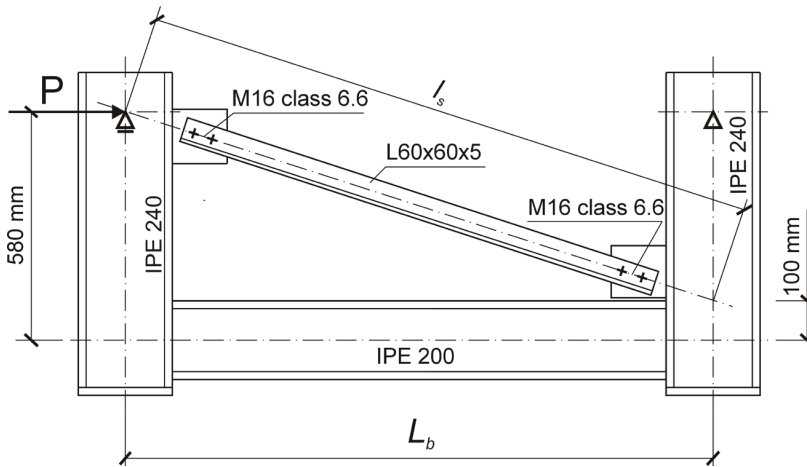


Fig. 9. Geometry of portal frame specimens of group BL (side view) [33].

Table 2

Symbols used to describe the group of tested frame specimens

Symbol of specimen		Lengths [mm]	
Groups	Subgroups	Beam system length L_b	Angle brace system length l_s
WL	WL 1320	1320	1405
	WL 1520	1520	1595
	WL 1925	1925	1985
BL	BL 1320	1320	1405
	BL 1520	1520	1595
	BL 1925	1925	1985

In addition, frames were held in the position in order to impose in-plane deformations only and to avoid frame out-of-plane instability. Two side beams were located at the top of columns, i.e. at the level of supports, restraining their end sections from out-of-plane displacements due to bending and torsion. Additional out-of-plane restraining points were located at the level of frame beam. Four side beams were used to mount one or two lateral restraints. The frame specimen with the shortest beam length had only one midspan lateral restraint while other two specimens with longer beam lengths were equipped with two lateral restraints equally spaced at 1/3 span length.

Table 3

Average values of mechanical properties from material tests of steel used for manufacturing of tested frame specimens

Profile	Specimen group	Strength [N/mm ²]			
		f_y		f_u	
		I	II	I	II
IPE 240	-	334		452	
IPE 200	-	303	330	424	454
L 60x60x5	WL	324	-	435	-
	BL 1320, BL1520	-	345	-	467
	BL 1925	324	-	435	-

I and II indicate the different delivery of mill rolled products for manufacturing of frame test specimens

4.2. MEASUREMENTS OF THE FORCE AND DEFORMATION OF ANGLE BRACE MEMBERS

All the tests were conducted in a static way for a monotonically increased horizontal load (up to the level of low stiffness of the tested specimen) and then for a monotonically increased horizontal displacement (when the limit point on the frame specimen load deformation characteristic was being reached and a descending branch of force-deformation characteristic observed to appear).

The member total shortening (Δ_w) being the superposition of the axial deformation and the deformation due to bow effect was measured directly by special LVDT devices (Figure 10).

The main purpose of tests conducted on braced frame specimens was firstly to get the experimental force-deformation characteristics of angle braces behaving in the frame specimen and secondly – the assessment of the influence of brace slenderness and different end connections on the brace effective length. The brace force was not measured directly but calculated in the postprocessing stage on the basis of strain measurements in the brace sections. Eight strain electro-resistant gauges were placed in close-to-end

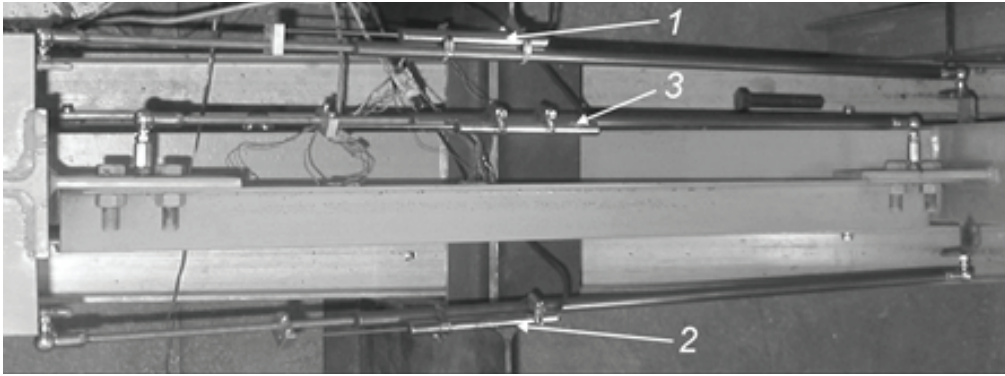


Fig. 10. Details of brace shortening measurement using LVDT devices mounted to a specimen of BL group; 1, 2 and 3 – LVDT devices [33].

brace sections (four at each brace end) and glued to external surfaces of both angle legs, approximately 10mm from the leg edges (Figure 11 shows the detail of one leg).

The measured strain components at each load level are used for the evaluation of stress blocks provided that linear strain relationship holds between the points where strains were measured. On the basis of this linear strain relationship, piecewise linear stress block patterns are then evaluated. In the elastic region of section response, the stress integration may be converted to the strain integration that were directly measured during tests. Thus the following relationship holds for the evaluation of the brace axial force:

$$(4.1) \quad N = \begin{cases} E \int \varepsilon dA & \text{for } |\varepsilon| \leq \varepsilon_y \\ f_y \int_A dA & \text{for } |\varepsilon| \geq \varepsilon_y \end{cases}$$

Moreover, the average strain value calculated from the four points in the top section of the brace angle (where the strain was measured experimentally) that is multiplied by the elasticity modulus and the approximate area of the angle section (two rectangles equal to the leg width and the leg thickness) shows to yield very good approximation of the brace axial force. The calculations of the axial force with this assumption is quite accurate in the elastic and moderate plastic strain regions. In the advanced permanent strain deformation region, the calculations were less accurate but this was the case after a large drop of the value of axial force with reference to the buckling strength level, therefore less important from the practical point of view.

The results of strain measurements recorded during tests and the stress blocks calculated according to Eq. (4.1) has been presented in [33].

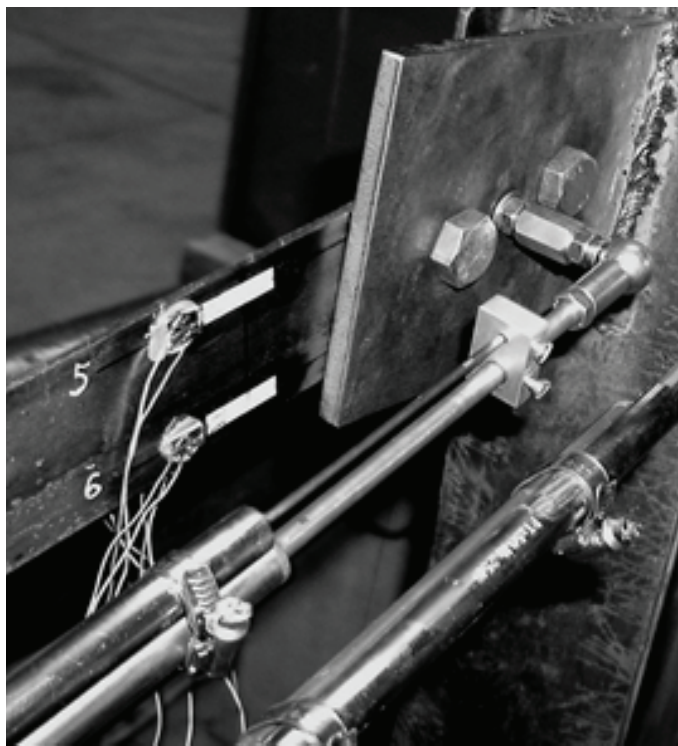


Fig. 11. Placement of electro-resistant gauges for monitoring close-to-edge point strains on one of the close-to-end side (the other two gauges are on the other side, therefore are invisible) [31].

4.3. EXPERIMENTAL RESULTS OF ANGLE BRACE BEHAVIOUR WITH REFERENCE TO BUCKLING STRENGTH AND EQUILIBRIUM PATH

It has been noted that for the braces that do not have distinctively different slenderness, there is no regularity in experimentally observed buckling strengths. It may lead to the situation that some of single experiments for the specimen with a longer brace length may give a lower value of the buckling strength than that obtained for a specimen with a shorter brace length, and vice versa, as it was observed in tests conducted by the author. This is less likely to be observed for braces in the specimens with a larger difference between the length of bracing members. The other source of differences in the ultimate strengths and postlimit traces of force-deformation characteristics of brace members might be attributed to the scatter of the steel yield stress that affected the evaluation of the first yield point.

It has been proven by Barszcz [32] that force-deformation characteristics $\bar{\sigma} - \bar{\varepsilon}$ of real angle braces with a single in-plane eccentricity (braces welded to the gusset plate)

and those with a space eccentricity (braces bolted to the gusset plate through one leg) are quite different. The stiffness degradation process takes place much faster in case of braces with a space eccentricity than for braces with a single in-plane eccentricity. The other important feature is that the latter exhibits less rapid drop in the force after reaching the ultimate strength than braces with a single in-plane eccentricity. The difference is mainly attributed to the following:

a) in the initial stage of loading, the faster reduction of the stiffness in case of bolt connected angle braces is attributed to the stronger influence of initial imperfections and to the effect of double eccentricity of the axial force that also results in a significantly lower ultimate strength of members connected through one leg in contrast to those welded and symmetrically connected to the gusset plate,

b) slower reduction of stiffness in the postlimit range is attributed to the effect of shear stresses due to torsion.

The direct comparison of results from an analytical formulation and experimental results for a single test involving instability is for civil engineering structures invaluable, since the buckling strength depends upon a number of factors among which the structural imperfections play an important role. It is therefore rational to compare the analytical formulation with the area representing the scatter of several test results, i.e. using two curves describing the envelope of test results. The other option is to use the lower bound curve predicted on the basis of probabilistic calculations, in case of representative number of tests enabling the statistical elaboration of results. Since the tests utilized in this paper count only three tests for each subgroup, the verification done in the following section utilizes the envelope of test results, therefore is directed towards the averaging of test results. In order to compare the influence of brace end connections on the behaviour of angle bracing members in WL and BL subgroups of tested frame specimens, the results are compared in one sketch for WL and BL specimens of the same subgroup. The comparison is presented in Figure 12. $N-A_w$ relationships are predicted in most cases with use of the axial force evaluation on the basis of experimental strain measurements on both end sections of brace members. Solid lines represent the curves obtained with use of measurements from gauges 1-4 in the section close to the top connection of the brace while the dotted lines illustrate the similar curves obtained with use of measurements from gauges 5-8 in the section close to the bottom connection of the brace.

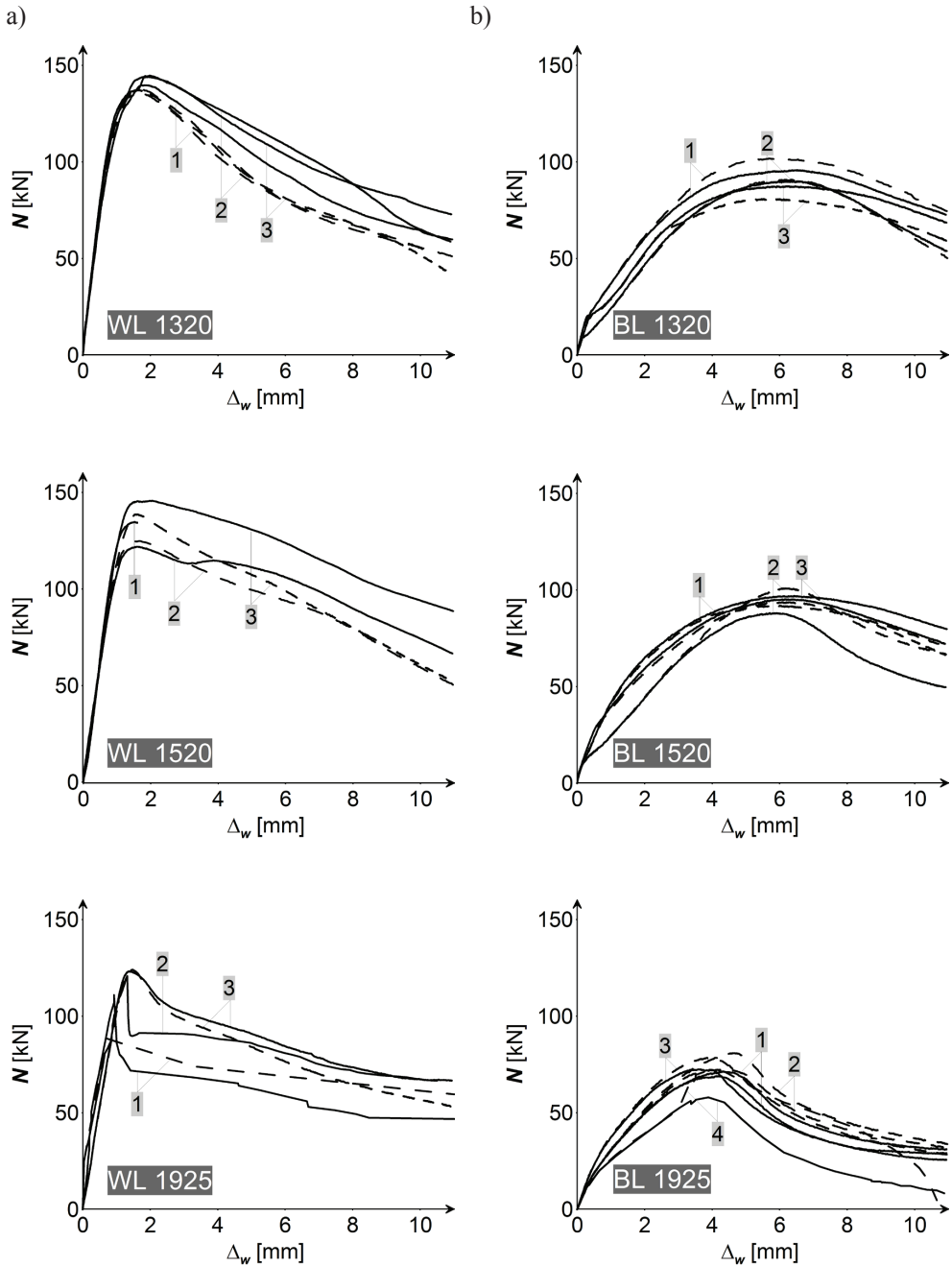


Fig. 12. Experimentally obtained force-deformation characteristics of bracing members, a) frame specimens WL, b) frame specimens BL; 1, 2, 3 and 4 – numbers of specimens [33].

5. VALIDATION OF ANALYTICAL FORCE-DEFORMATION CHARACTERISTIC OF ANGLE BRACE

Experimental investigations carried out for frame specimens of WL type and for the same number of BL specimen types have shown that there were substantial differences existing between the behavior of steel angle braces with regard to welded end connections and bolted end connections (see Figure 12). The differences are not only due to type of the connector but predominantly due to the type of eccentricity (in-plane or space) and the different effect of imperfections in both types of angle bracing members. It has generally been proven that angles with bolted connections are weaker, i.e. exhibit the lower buckling strength and lower placement of force-deformation characteristics than those corresponding to their welded counterparts. It brings one to the conclusion that the calibration of analytical model parameters needs to be done separately for both groups of bracing members. The effective length factors of bracing members were chosen on the assumption of different values for both groups, namely for welded braces $\mu=0,5$ while for bolted braces $\mu=1,0$. Different effective length factors of bracing members result from the different behaviour of two groups of angle braces in frame specimens. In case of braces with welded connections the effective length was shifted towards the theoretical value for a rigidly connected element. The brace tended to buckle in the frame plane thus the gusset plate exhibited a large rotational stiffness. Contrary, in case of braces with bolted connections the effective length was shifted towards the theoretical value for a nominally pinned element. The brace tended to deform also out of the frame plane where the gusset plate exhibited much smaller rotational stiffness.

The effect of geometric imperfections are integrally accounted for in modelling of braces in the value of model parameter $n=5$ for welded and $n=3,5$ for bolted braces. The effect of elastic initial stiffness EA reduction is not considered for fork welded connections ($\psi=1,0$). For braces with bolted connections the effect of torsion on the reduction of the elastic initial stiffness EA plays an important role so that the model parameter ψ was taken as less than unity and dependent upon the member slenderness ratios as in Eqn. (2.10):

$$\psi = \frac{0,2}{\left[0,2 + 1,4 \left(\frac{\bar{\lambda}_{Te}}{\bar{\lambda}_F} \right)^2 \right]}$$

where $\bar{\lambda}_{Te}^2 \geq \bar{\lambda}_T^2$, $\bar{\lambda}_{Te}$, $\bar{\lambda}_T$, $\bar{\lambda}_F$ – slenderness ratios corresponding to forces N_{Te} , N_T and N_F , respectively.

Comparison of experimental force-deformation curves and analytical curves constructed with use of model parameters evaluated to fit the laboratory tests are presented in Figure 13a) for angles of WL type, and in Figure 13b) for angles of BL type. All the model parameters that do not present in Figure 13 are listed in Table 4.

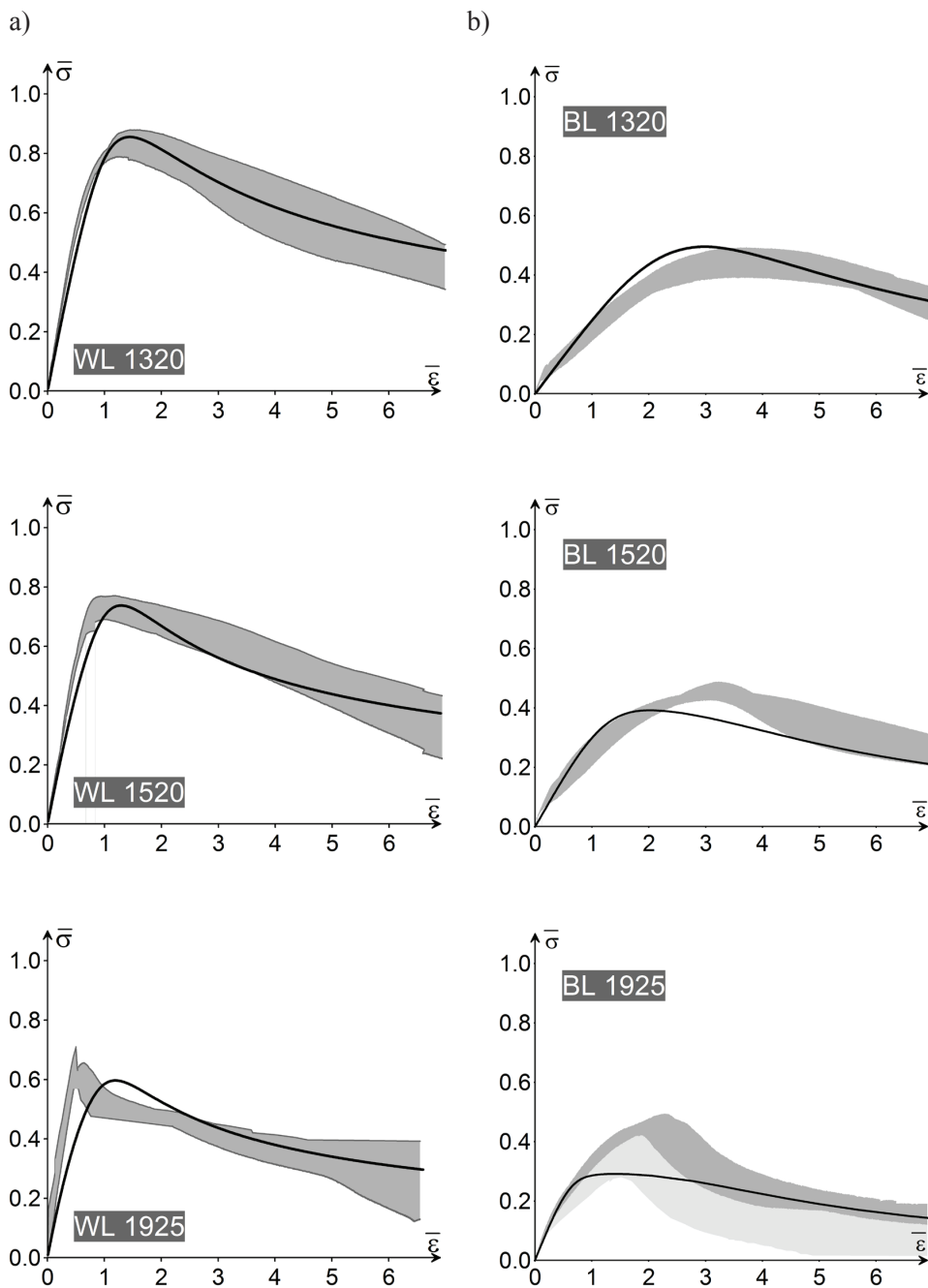


Fig. 13. Comparison of analytical force-deformation characteristic with experimental envelope of results:
a) WL type braces, b) BL type braces.

Table 4

Parameters of analytical models describing force-deformation characteristics of compressed bracing members in tested frame specimens

Symbol of specimen group	Actual length l (between the gravity centers of end connections) [mm]	Buckling length factor	Relative slenderness ratios			Model parameters		
		μ_v ¹⁾	$\bar{\lambda}_{cr}$	$\bar{\lambda}_F$	$\bar{\lambda}_{Te}(\bar{\lambda}_r)^2$	a_u	m	ψ
WL 1320	952	0,50	0,59	0,47	0,47 (0,66)	1,7	0,5	1
WL 1520	1145		0,70	0,60	0,49 (0,70)			1
WL 1925	1545		0,84	0,77	0,47 (0,67)			1
BL 1320	960	1,00	1,24	1,05	0,68 (0,74)	0,4	1,0	0,25
BL 1520	1170		1,45	1,29				0,34
BL 1925	1565		1,68	1,57	0,62 (0,68)			0,47

¹⁾ Buckling length factor μ_v taken as unity
²⁾ $\bar{\lambda}_{Te}, \bar{\lambda}_r$ – different for different specimen groups evaluated for actual values of eccentricities and yield stress averaged from gauge records of each specimen groups of WL and BL types

For experimental generalized force-deformation characteristics, the experimental envelope of results obtained from individual 3 tests for each specimen group (identical beam length and joint type) is used. The area enclosed by the upper and lower boundary lines of the envelope that is utilized for the calibration exercise refers to dark grey colour. The scatter of experimental characteristics was the greatest in case of bolted longest angle. The light gray colour refers to the experimental characteristic that is placed much lower than the other two indicated by the area bounded by the dark grey colour. This result was considered also reliable since the pilot tests have also indicated lower placement of the angle force-deformation of the specimen with the longest beam length. It is noticeable that the analytical formulation developed herein and applied together with calibrated model parameters leads to a prediction of the experimental characteristics accurate enough for both welded and bolted angle braces.

6. CONCLUDING REMARKS

Modelling of the force-deformation characteristic of single angle members of vertical truss bracings is dealt with in this paper. The analytical approach based on the Murzewski's method of statistical hypothesis that had been used by the author in earlier studies for the construction of buckling curves and force-deformation characteristics of axially loaded compression members is further developed in this paper to account for eccentricities of member end connections. Two different boundary conditions, typical for engineering practice, are dealt with, namely corresponding with fork welded

(with in-plane eccentricity) and lap bolted through one leg (with space eccentricity). Experimental program of testing the behaviour of angle braces in portal sub-frame specimens was described together with the presentation of test results. The main purpose of tests conducted on portal braced frame specimens was firstly to get the experimental force-deformation characteristics of angle braces behaving in the frame specimen and secondly – to assess the influence of brace slenderness and different end connections on the brace effective length. It has been proven that the force-deformation characteristics $\bar{\sigma} - \bar{\varepsilon}$ of real angle braces with a single in-plane eccentricity (braces welded to the gusset plate) and those with a space eccentricity (braces bolted to the gusset plate through one leg) are quite different. The stiffness degradation process takes place much faster in case of braces with a space eccentricity than for braces with a single in-plane eccentricity. The other important feature is that the latter exhibits less rapid drop in the force after reaching the ultimate strength than braces with a single in-plane eccentricity. The difference is mainly attributed to the following:

a) in the initial stage of loading, the faster reduction of the stiffness in case of bolt connected angle braces is attributed to the stronger influence of initial imperfections and to the effect of double eccentricity of the axial force that results in a significantly lower ultimate strength of members connected through one leg in contrast to those welded and symmetrically connected to the gusset plate,

b) slower reduction of stiffness in the postlimit range is attributed to the effect of shear stresses due to torsion.

Results of experimental investigations were used for the calibration of developed analytical model of the brace behaviour. It is emphasized that different analytical formulations need to be postulated for two different conditions of brace end connections. Such formulations are presented in this paper and their model parameters are calibrated on the basis of experimental data. It was found that there is a need for two sets of model parameters calibrated independently for two different groups of angle braces, namely for welded and bolted angle braces. The two sets of calibrated parameters for analytical curves best fitting the experimental results are not close to each other. In order to postulate a generalized set of model parameters covering all the members sizes, eccentricities and slenderness ratios, a wider experimental investigations are needed. It is however quite clear that the proposed analytical model for the description of force-deformation characteristics of eccentrically connected angle braces is very useful since it allows for an accurate reproduction of experimental force-deformation characteristics.

The developed brace model is to be implemented to the computer code for the advanced analysis of semi-rigid steel frameworks designed according to the limit states concept.

Acknowledgements

Investigations were carried out within the financial support provided by the Ministry of Science and Higher Education within statutory grants of the Faculty of Civil Engi-

neering of the Warsaw University of Technology designated in the consecutive years 2006-2012. Experimental work was conducted at the Structures Laboratory of the Metal Structures Division of the above stated Faculty. The assistance provided by laboratory staff members under the leadership of Mr. Jan Witkowski and Mr. Włodzimierz Sotomski is highly appreciated. Certain aspects of modelling of the dimensionless member force-deformation characteristic of angle brace members were initially discussed in the author's conference papers cited in references.

REFERENCES

1. N. S. TRAHAIR, T. USAMI, T. V. GALAMBOS, Eccentrically Loaded Single Angle Columns. Research Report No. 11, Department of Civil and Environmental Engineering, Washington University, St. Couris, 1969.
2. M. C. TEMPLE, S. S. SAKALA, Single angle compression members welded by one leg to a gusset plate. Experimental study. Canadian Journal of Civil Engineering, vo. 25, no. 3, 569-584, 1988.
3. D. H. ELGAALY, W. DAWIDS, Behavior of single angle compression members. Journal of Structural Engineering, ASCE, vol. 117, no. 12, 3720-3741, 1991.
4. S. M. R. ALDURI, M. K. S. MAGUDULA, Flexural buckling of steel angles. Experimental investigations. Journal of Structural Engineering, ASCE, vol. 122, no. 3, 309-317, 1996.
5. S. L. CHAN, S. H. CHO, Second-order analysis and design of angle trusses. Part I: Elastic analysis and design. Engineering Structures, vol. 30, no. 3, 616-625, 2008.
6. R. D. ZIEMIAN, Guide to Stability Design Criteria for Metal Structures. 6th Edition, John Wiley & Sons, 2010.
7. M. A. GIŻEJOWSKI, A. M. BARSZCZ, J. D. G. FOSTER, J. UZIĄK, O. J. KANYETO, Experimental investigations of the behaviour of angle struts, Proceedings of the XIth ICMS-2006 (eds. M. Giżejowski, A. Kozłowski, J. Ziółko), Taylor&Francis, Rzeszów, Poland, 152-153, 2006 [full paper on CD, 145-154].
8. Y. LUI, S. CHANTEL, Experimental study of steel single unequal leg angles under eccentric compression. Journal of Constructional Steel Research, vol. 67, no. 6, 919-928, 2011.
9. S. CHEN, X. WANG, Buckling Strength of Single Angle Struts. Part 1: Angles Subject to Axial Compression. Advances in Structural Engineering, vol. 16, no. 6, 1129-1137, 2013.
10. S. CHEN, X. WANG, Buckling Strength of Single Angle Struts. Part 2: Angles Connected by One Leg at Both Ends. Advances in Structural Engineering, vol. 16, no. 6, 1139-1148, 2013.
11. K. IKEDA, S. A. MAHIN, Cyclic response of steel braces, Journal of Structural Engineering, 112, 2, 242-261, 1986.
12. W. GAN, J. F. HALL, Static and dynamic behavior of steel braces under cyclic displacements, Journal of Engineering Mechanics, 124, 1, 87-93, 1998.
13. J. JIN, S. EL-TAWIL, Inelastic cyclic model for steel braces, Journal of Engineering Mechanics, 129, 5, 548-577, 2003.
14. B. V. FELL, A. M. KANVINDE, G. G. DEIERLEIN, A. T. MYERS, Experimental investigation of inelastic cycling buckling and fracture of steel braces, Journal of Structural Engineering, 135, 1, 19-22, 2009.
15. A. DAVARAN, M. ADELZADEH, An improved non-linear physical modeling method for brace elements. Transaction A: Civil Engineering, Scientia Iranica, 16, 1, 58-64, 2009
16. M. ŁUBIŃSKI, J. KARCEWSKI, J. KAFARSKI, Limit-state-design of spatial lattice structures. Archiwum Inżynierii Łądowej, XII, 1, 27-41, 1976 [in Polish].
17. A. M. BARSZCZ, Load carrying capacity of space deck member accounted for shakedown effects, Warsaw University of Technology, Warszawa 1988 [manuscript in Polish].

18. J. KARCEWSKI, A. BARSZCZ, A large deflections analysis of an elastic-plastic strut axially loaded in a cyclically variable manner, Archives of Civil Engineering, XLI, 2, 244-265, 1995.
19. S. KATO, M. FUJIMOTO, T. OGAWA, Buckling load of steel single-layer reticulated domes of circular plan. Journal of the International Association for Shell and Spatial Structures. Vol. 46, No. 1, 41-63, 2005.
20. T. OGAWA, S. KATO, M. FUJIMOTO, Buckling load of elliptic and hyperbolic paraboloidal steel single-layer reticulated shells of rectangular plan. Journal of the International Association for Shell and Spatial Structures. Vol. 49, No. 1, 21-36, 2008.
21. A. STEINBOECK, G. HOEFINGER, X. JIA, H.A. MANG, Three pending questions in structural stability. Journal of the International Association for Shell and Spatial Structures. Vol. 50, No. 1, 51-64, 2009.
22. G. MONTI, C. NUTI, Nonlinear cyclic behavior of reinforcing bar including buckling, Journal of Structural Engineering, 118, 12, 3268-3284, 1992
23. R. DHAKAL, K. MAEKAWA, Path-dependent cyclic stress-strain relationship of reinforcing bar including buckling, Engineering Structures, 24, 11, 1383-1396, 2002
24. J. KORENZ, Modeling of reinforcing bar subjected to cyclic loading in inelastic range. Przegląd Budowlany, nr 5, 141-143, 2012 [in Polish].
25. J. MURZEWSKI, Theory of random load carrying capacity of rod structures, Studia z Zakresu Inżynierii, Nr. 15, KILiW PAN-PWN, Warszawa 1976 [in Polish].
26. A. M. BARSZCZ, M.A. GIZEJOWSKI, A generalized M-R-M approach for modelling of the stability behaviour of imperfect steel elements and structures, Archives of Civil Engineering, 52, 1, 59-85, 2006.
27. A. M. BARSZCZ, M.A. GIZEJOWSKI, An Equivalent Stiffness Approach for Modeling the behavior of Compression Members According to Eurocode 3, Journal of Constructional Steel Research, 63, 1, 55-70, 2007.
28. PN-3200/B-03200: Steel structures: Static calculations and design. PKNMiJ; Warszawa 1994.
29. EN 1993-1-1, Eurocode 3: Design of steel structures. Part 1-1: General rules and rules for buildings, Brussels: CEN, 2005.
30. A. BARSZCZ, M. GIZEJOWSKI, Buckling modes and computational models of compressed bracing members. Inżynieria i Budownictwo, nr 9, 497-502, 2013 [in Polish].
31. A. M. BARSZCZ, Modelling and experimental investigations of the behaviour of angle bracing strut in steel frame. Proceedings of Local Seminar of IASS Polish Chapter: Lightweight Structures in Civil Engineering [ed. J.B. Obrębski], Warsaw: Micro-Publisher, 106-113, 2007.
32. A. M. BARSZCZ, Experimental investigations of braced frame system, Inżynieria i Budownictwo, nr 7, 380-384, 2010 [in Polish].
33. A. M. BARSZCZ, Investigation into the modelling of angle brace member. Proceedings of Local Seminar of IASS Polish Chapter: Lightweight Structures in Civil Engineering [ed. J.B. Obrębski], Warsaw: Micro-Publisher, 54-65, 2012.

Received: 14.12.2013

Revised: 27.02.2014

Appendix: Solution of the cubic algebraic equation and its first derivative for the dimensionless force-deformation characteristic.

This paper contains several references to the closed form solution of third degree algebraic equation describing different problems referred to force-deformation characteristic and buckling forces of asymmetric brace section members that has the following form:

$$ax^3 + bx^2 + cx + d = 0$$

The real roots of the above equation are expressed as follows:

$$x = \begin{cases} -2r \cos \frac{\varphi}{3} - \frac{b}{3a}, & 2r \cos \frac{\pi - \varphi}{3} - \frac{b}{3a}, & 2r \cos \frac{\pi + \varphi}{3} - \frac{b}{3a} & \text{if } p \leq 0 \quad D \leq 0 \\ -2r \cosh \frac{\varphi}{3} - \frac{b}{3a} & & & \text{if } p \leq 0 \quad D > 0 \\ -2r \sinh \frac{\varphi}{3} - \frac{b}{3a} & & & \text{if } p > 0 \end{cases}$$

where φ is derived from the relationships:

$$\cos \varphi = \frac{q}{r^3} \quad \text{if } p \leq 0 \quad \text{and } D \leq 0$$

$$\cosh \varphi = \frac{q}{r^3} \quad \text{if } p \leq 0 \quad \text{and } D > 0$$

$$\sinh \varphi = \frac{q}{r^3} \quad \text{if } p > 0$$

$$p = \frac{3ac - b^2}{9a^2}, \quad q = \frac{2b^3}{54a^3} - \frac{bc}{6a^2} + \frac{d}{2a}, \quad D = q^2 + p^3.$$

In the above equations $r = \pm \sqrt[3]{p}$, while the sign of r should follow the sign of q .

In case of force-deformation characteristic $\bar{\sigma}_E - \bar{\varepsilon}$, the unknown x becomes $\bar{\sigma}_E$, and only the coefficient a is a constant while the other coefficients b , c and d are the functions of $\bar{\varepsilon}$. Hence the stiffness degradation factor of considered dimensionless elastic second order force-deformation characteristic can be written down in the following format:

$$\bar{\kappa}_E = \frac{d\bar{\sigma}_E}{d\bar{\varepsilon}} = \left\{ \begin{array}{l} 2r' \cos \frac{\varphi}{3} + \frac{2}{3} r\varphi' \sin \frac{\varphi}{3} - \frac{b'}{3a} \\ \text{lub } 2r' \cos \frac{\pi - \varphi}{3} + \frac{2}{3} r\varphi' \sin \frac{\pi - \varphi}{3} - \frac{b'}{3a} \\ \text{lub } 2r' \cos \frac{\pi + \varphi}{3} - \frac{2}{3} r\varphi' \sin \frac{\pi + \varphi}{3} - \frac{b'}{3a} \end{array} \right\} \text{if } p \leq 0 \text{ and } D \leq 0$$

$$-2r' \cosh \frac{\varphi}{3} - \frac{2}{3} r\varphi' \sinh \frac{\varphi}{3} - \frac{b'}{3a} \quad \text{if } p \leq 0 \text{ and } D > 0$$

$$-2r' \sinh \frac{\varphi}{3} - \frac{2}{3} r\varphi' \cosh \frac{\varphi}{3} - \frac{b'}{3a} \quad \text{if } p > 0$$

where:

$$\varphi' = \frac{d\varphi}{d\bar{\varepsilon}} = \left\{ \begin{array}{l} \frac{d\left(\arccos \frac{q}{r^3}\right)}{d\bar{\varepsilon}} = \frac{3qr' - rq'}{r\sqrt{r^6 - q^2}} \quad \text{if } p \leq 0 \text{ and } D \leq 0 \\ \frac{d\left(\arccos h \frac{q}{r^3}\right)}{d\bar{\varepsilon}} = \frac{rq' - 3qr'}{r\sqrt{q^2 - r^6}} \quad \text{if } p \leq 0 \text{ and } D > 0 \text{ and } \frac{q}{r^3} \geq 1 \\ \frac{d\left(\arcsin h \frac{q}{r^3}\right)}{d\bar{\varepsilon}} = \frac{rq' - 3qr'}{r\sqrt{r^6 + q^2}} \quad \text{if } p > 0 \end{array} \right.$$

$$r' = \left\{ \begin{array}{l} \pm \frac{p'}{2\sqrt{p}} \quad \text{if } p > 0 \\ \mp \frac{p'}{2\sqrt{-p}} \quad \text{if } p < 0 \end{array} \right.$$

The upper sign is applied when while the bottom one when . Moreover, the following notation is used:

$$p' = \frac{3ac' - 2bb'}{9a^2}, \quad q' = \frac{b^2b'}{9a^3} - \frac{b'c + bc'}{6a^2} + \frac{d'}{2a}.$$